Manuscript prepared for Atmos. Chem. Phys.
with version 2015/04/24 7.83 Copernicus papers of the LaTeX class copernicus.cls.
Date: 18 March 2016

Exploring atmospheric blocking with GPS radio occultation observations

Lukas Brunner[1, 2], Andrea K. Steiner[1, 2, 3], Barbara Scherllin-Pirscher[1, 3], and Martin W. Jury[1]

[1]Wegener Center for Climate and Global Change (WEGC), University of Graz, Graz, Austria
[2]FWF-DK Climate Change, University of Graz, Graz, Austria
[3]Institute for Geophysics, Astrophysics, and Meteorology/Institute of Physics, University of Graz, Graz, Austria

Correspondence to: Lukas Brunner (lukas.brunner@uni-graz.at)

Abstract. Atmospheric blocking has been closely investigated in recent years due to its impact on weather and climate, such as heat waves, droughts, and flooding. We use, for the first time, satellite-based observations from Global Positioning System (GPS) radio occultation (RO) and explore their ability to resolve blocking in order to potentially open up new avenues complementing models and re-analyses. RO delivers globally available and vertically high resolved profiles of atmospheric variables such as temperature and geopotential height (GPH). Applying a standard blocking detection algorithm we find that RO data robustly capture blocking as demonstrated for two well-known blocking events over Russia in summer 2010 and over Greenland in late winter 2013. During blocking episodes, vertically resolved GPH gradients show a distinct anomalous behavior compared to climatological conditions up to 300 hPa and sometimes even further up to the tropopause. The accompanied increase in GPH of up to 300 m in the upper troposphere yields a pronounced tropopause height increase. Corresponding temperatures rise up to 10 K in the middle and lower troposphere. These results demonstrate the feasibility and potential of RO to detect and resolve blocking and in particular to explore the vertical structure of the atmosphere during blocking episodes. This new observation-based view is available globally at the same quality so that also blocking in the Southern Hemisphere can be studied with the same reliability as in the Northern Hemisphere.

1 Introduction

Weather and climate in the Northern Hemisphere (NH) mid-latitudes are dominated by large-scale circulations of the atmosphere and ocean, and dynamical features including jet streams, storm tracks, and blocking. Blocking describes an atmospheric situation where a persistent and stationary high pressure system blocks the climatological westerly flow for several days to weeks (Rex, 1950). It is often associated with anomalous weather patterns and extreme events (e.g., Cattiaux et al., 2010; Matsueda, 2011; Mattingly et al., 2015). The blocking over Russia in summer 2010, for instance,

was one of the strongest blocking events in recent history with impacts on large parts of Europe and Asia. It did not only lead to record-breaking temperatures in Russia but also has been associated with severe flooding in Pakistan at the same time (Matsueda, 2011; Galarneau Jr. et al., 2012). Severe impacts of these blocking-related extremes on society and economy have increased the interest in investigating blocking evolution and impacts of climate change on blocking frequency and duration (Sillmann et al., 2011; Cohen et al., 2014; Shepherd, 2014; Gramling, 2015; Lhotka and Kyselý, 2015).

In the NH blocking preferentially occurs near the north-eastern ends of the Atlantic and Pacific storm tracks (Euro-Atlantic blocking and North Pacific blocking, respectively) (Doblas-Reyes et al., 2002; Barriopedro et al., 2010; IPCC, 2013). Blocking is connected to the North Atlantic oscillation and to jet stream variability (e.g., Scherrer et al., 2006; Davini et al., 2014a). A connection of blocking to stratospheric phenomena such as sudden stratospheric warming events has been suggested by several authors in the past (e.g., Quiroz, 1986; Martius et al., 2009; Woollings et al., 2010; Barriopedro and Calvo, 2014). Recently, also thermodynamic processes in the troposphere such as latent heating were found important for the formation of blocking (Pfahl et al., 2015).

In the Southern Hemisphere (SH) where the mid-latitudes are mostly characterized by oceanic regions with very sparse human population, blocking has received less attention. Main blocking regions are located in the Australian-New Zealand area and in the southeast Pacific (Lejenäs, 1984; Mendes et al., 2008). Frequency and location of SH blocking are strongly influenced by the El Niño–Southern Oscillation (ENSO) and the southern annular mode (Wiedenmann et al., 2002; Oliveira et al., 2014). However, sparse coverage by classical observational systems in the SH introduces larger uncertainties into SH blocking research (Tibaldi et al., 1994; Marques and Rao, 2000).

Most blocking studies are based on climate model output or re-analysis data analyzing geopotential height (GPH) fields at a constant pressure level (e.g., Barriopedro et al., 2006, 2010; Barnes et al., 2014; Davini et al., 2014b). Other studies employed dynamical atmospheric parameters such as vertically averaged potential vorticity or potential temperature on the dynamical tropopause (e.g., Pelly and Hoskins, 2003; Schwierz et al., 2004). However, it has been shown that the blocking frequency exhibits considerable inter-model spread in current climate models (Anstey et al., 2013; IPCC, 2013) and blocking trends can differ depending on the re-analysis used (Barnes et al., 2014).

We use, for the first time, observations from Global Positioning System (GPS) radio occultation (RO) to detect blocking and inspect the atmospheric structure during blocking events. This study does not provide an analysis of blocking dynamics nor an extended comparison to model or re-analysis data. Our objective is to explore the feasibility of detecting blocking and characterize its three-dimensional structure with RO observations. To this end we show blocking patterns and the vertically resolved structure of the troposphere and lower stratosphere during two well known blocking events: the blocking over Russia in summer 2010 and the blocking over Greenland in winter 2013.

2 Radio occultation data

The analysis presented here is based on RO measurements. RO is a satellite-based limb sounding technique, delivering profiles of atmospheric parameters with global coverage and high vertical resolution of about 100 m in the troposphere to 1.5 km in the stratosphere (Kursinski et al., 1997; Gorbunov et al., 2004). The horizontal resolution ranges from about 60 km to 300 km (Kursinski et al., 1997). RO data are of high quality. In the troposphere the accuracy of GPH is about 10 m and of temperature less than 1 K (Scherllin-Pirscher et al., 2011b), with averaged profiles exhibiting further statistical reduction of errors (Scherllin-Pirscher et al., 2011a). Structural uncertainty is low and data from different satellites are highly consistent and require no inter-satellite calibration (Foelsche et al., 2011; Ho et al., 2012; Steiner et al., 2013).

RO data are of high benefit for improving weather forecasts and atmospheric analyses (note that several weather prediction centers already assimilate RO data) as well as for monitoring atmospheric climate variability and changes (see, e.g., Anthes, 2011; Steiner et al., 2011; Gleisner et al., 2015; Randel and Wu, 2015). RO has been applied, so far, for a range of atmospheric dynamics studies, such as investigating the planetary boundary layer (e.g., von Engeln et al., 2005) and tropopause (Schmidt et al., 2008; Rieckh et al., 2014; Peevey et al., 2014), the ENSO (Scherllin-Pirscher et al., 2012; Sun et al., 2014), atmospheric tides (Pirscher et al., 2010), and waves including the Quasi-Biennial Oscillation (Randel et al., 2003; Schmidt et al., 2005), Kelvin waves (e.g., Randel and Wu, 2005), and stratospheric gravity waves (e.g., de la Torre and Alexander, 2005; Tsuda, 2014). Recent studies also focused on tracing wind fields (Scherllin-Pirscher et al., 2014) and analyzing the thermodynamic structure during cyclones (Biondi et al., 2015).

RO data used in the present study were processed with the Wegener Center occultation processing system version 5.6 (OPSv5.6) (Schwärz et al., 2013). The full set of atmospheric variables derived from RO includes density, pressure, GPH, temperature, potential temperature, and tropospheric water vapor. Observations from several RO missions are exploited including CHAMP, GRACE, and COSMIC for the period 2006 to 2013, where we focus on two well-known blocking events: over Russia in summer 2010 (Russian blocking) and over Greenland in late winter/early spring 2013 (Greenland blocking). During these time periods about 800 high quality RO profiles are available per day in the NH.

We analyze GPH and temperature profiles as a function of pressure. The levels of the pressure grid have been calculated from $p_i(z_i) = p_0 \exp(-\frac{z_i}{H})$, with $p_0 = 1013.25$ hPa (standard surface pressure), $H = 7000$ m (constant scale height), and altitude z_i ranging from the surface to 16 km (corresponding to about 100 hPa) in equidistant 200 m steps.

We calculate daily fields on a $2.5^\circ \times 2.5^\circ$ longitude-latitude grid by applying a weighted average to the RO profiles:

$$x_{\mathrm{grid}}(\lambda, \phi, d) = \frac{\sum_i w_i x_i(\lambda', \phi', d')}{\sum_i w_i},$$

where $x_{\mathrm{grid}}(\lambda, \phi, d)$ is GPH or temperature at a specific grid point at longitude λ, latitude ϕ, and day d. $x_i(\lambda', \phi', d')$ denotes an individual atmospheric profile at RO event location λ', ϕ', and day d'. All RO events within $\pm 7.5^\circ$ in longitude, $\pm 2.5^\circ$ in latitude, and ± 2 days are considered and weighted with a Gaussian weighting function w_i over longitude and time according to $w_i = \exp\left(-\left[\left(\frac{\Delta\lambda}{L}\right)^2 + \left(\frac{\Delta d}{D}\right)^2\right]\right)$, with $L = 7.5^\circ$ and $D = 1$ day (adapted from Randel and Wu (2005)). This effective resolution has been chosen to minimize the number of bins in which no measurements exist, while still resolving most of the atmospheric variability. Sensitivity tests with data from the European Centre for Medium-range Weather Forecasts (ECMWF) re-analysis Interim (ERA-Interim) (Dee et al., 2011) showed only small differences (< 100 m in geopopotential height) between mean fields obtained from this binning and native $2.5^\circ \times 2.5^\circ$ daily fields, confirming the robustness of our gridding strategy.

Figures 1a and 2a depict the distribution of RO profiles and the number of profiles contributing to each grid cell for two exemplary days during the Russian blocking in 2010 and the Greenland blocking in 2013, respectively. More than 80 % of all grid cells contain information of at least four RO profiles. Only near the equator and at very high latitudes the number of profiles decreases and some grid cells with no measurements exist.

Applying our gridding method, we are able to resolve synoptic-scale atmospheric variability on a daily basis as shown for GPH at the 500 hPa pressure level (Fig. 1b and 2b). At mid-latitudes (between approximately 45°N and 65°N), mean GPH fields reveal high-pressure systems over Scandinavia and the western part of Russia in summer 2010 (Russian blocking) and over the East-Atlantic in winter/spring 2013 (Greenland blocking), representing typical blocking situations (Davini et al., 2014a).

These features are even more pronounced in GPH anomaly fields (Fig. 1c and 2c) which are calculated relative to the daily means averaged over 8 years (2006 to 2013). GPH anomalies are larger during the Greenland blocking ($>$300 m) in winter than during the Russian blocking (mainly within 200 m) in summer. However, both anomalies are distinctively larger than the variability shown as standard deviation of the individual RO profiles in each grid cell in Fig. 1d and 2d for the Russian and Greenland blocking, respectively.

To provide information about uncertainty associated with discrete data sampling and our averaging method, Fig. 1e and 2e show the sampling error (SE). It is calculated as the difference between the mean field from co-located ECMWF analysis profiles applying the same averaging technique as for RO profiles (see above) and the daily mean ECMWF analysis field on a native $2.5^\circ \times 2.5^\circ$ resolution. For both blocking events, the SE is distinctively smaller than the GPH anomalies. It is slightly larger during the Greenland blocking than during the Russian blocking because (i) atmospheric variability is stronger in the winter season than in the summer season and (ii) the number of profiles is slightly smaller in 2013 than in 2010. However, the small magnitude of the SE (Fig. 1e and 2e) compared to blocking-related anomalies (Fig. 1c and 2c) as well as small standard deviation (Fig. 1d and 2d)

underpins that RO data sampling is sufficient to capture atmospheric variability on a daily basis when applying a suitable averaging technique. RO data are therefore well suited for blocking detection.

3 Blocking detection

Blocking diagnosis is usually performed on a fixed pressure level (e.g., Barriopedro et al., 2006, 2010; Barnes et al., 2014; Davini et al., 2014b). To detect blocking episodes we utilize a frequently used blocking index based on GPH at 500 hPa (Tibaldi and Molteni, 1990; Scherrer et al., 2006; Davini et al., 2012, 2014b). Blocking is identified via three criteria.

First, the northern and southern GPH gradients, ΔZ_{N} and ΔZ_{S}, are calculated as

$$\Delta Z_{\mathrm{N}}(\lambda,\phi,p) = \frac{Z(\lambda,\phi+\Delta\phi,p) - Z(\lambda,\phi,p)}{\Delta\phi},$$
$$\Delta Z_{\mathrm{S}}(\lambda,\phi,p) = \frac{Z(\lambda,\phi,p) - Z(\lambda,\phi-\Delta\phi,p)}{\Delta\phi},$$

where $\Delta\phi = 15°$. The computation is performed separately for each $2.5° \times 2.5°$ grid point from $50°$N to $65°$N, thus grid points are effectively used from $35°$N to $80°$N over all longitudes. Following Davini et al. (2014a), *instantaneous blocking (IB)* is identified if both of the following conditions are met: $\Delta Z_{\mathrm{S}}(\lambda,\phi,p') > 0\,\mathrm{m/^{\circ}lat}$ and $\Delta Z_{\mathrm{N}}(\lambda,\phi,p') < -10\,\mathrm{m/^{\circ}lat}$ at $p' = 500$ hPa. A positive southward gradient indicates the reversal of the meridional GPH gradient with easterlies equatorward of ϕ. This is the essential condition for blocking. Additionally, the second condition indicates strong westerlies poleward of ϕ. It rules out some synoptic cases which marginally satisfy condition one but are no blockings (Tibaldi and Molteni, 1990; Anstey et al., 2013).

The second blocking detection criterion is set to account only for large high-pressure systems. Thus, *extended IB* is identified at a grid point, if all neighboring grid cells within $\pm 7.5°$ longitude are instantaneously blocked.

The third criterion guarantees to detect only stationary high-pressure systems and to filter out fast moving events. It specifies that a grid cell with extended IB is *blocked*, if at least one grid cell with extended IB is found within a box of $10°$ longitude $\times$ $5°$ latitude on each of the neighboring ± 2 days.

Figure 3 shows the blocking occurrence and temporal evolution at the 500 hPa pressure level for the Russian and Greenland blocking, respectively. To demonstrate the influence of the three blocking criteria, Fig. 3 also includes IB and extended IB. Note the very similar patterns for all criteria, indicating that the gradient criterion (first criterion) is in principle sufficient for catching most of the blocking features.

Overall, the evolutions of the blocking patterns are different for the Russian blocking and the Greenland blocking. While the Russian blocking is more continuous, lasting for more than six weeks from end of June to mid-August, the Greenland blocking is most pronounced only for about two weeks from mid-February to early March, with minor and less extended blockings taking place until

mid-April 2013. The Russian blocking is smaller in longitudinal extent ranging over 55° while the Greenland blocking is twice as large ranging over 100° in longitude.

We compared the resulting blocking patterns from RO observations to those from ERA-Interim data and found very good agreement (Brunner et al., 2015). The consistency of our results is also confirmed by comparison to existing literature (e.g., Matsueda, 2011, Fig.1b). This furthermore proves the feasibility of blocking detection with RO.

4 Vertically resolved blocking patterns

Tropospheric profiles of GPH gradients are shown in Fig. 4 for two exemplary days and regions for the Russian and Greenland blocking, respectively. Climatological GPH gradients in the same region are additionally shown for comparison. These climatological gradients ΔZ_{S} and ΔZ_{N} for June-July-August (JJA) and February-March-April (FMA) are obtained from averaging over all available years (2006 to 2013).

During normal, climatological conditions (Fig. 4a,b), all gradient profiles are close to each other. In the entire troposphere above the boundary layer GPH gradients are smaller than 0 m/°lat indicating the climatological westerly geostrophic flow at NH mid-latitudes. In general, the climatological northern gradients are near to the blocking threshold (-10 m/°lat). For the inspected regions they are even found below the threshold.

A clear separation between the northern and southern gradients can be observed during blocking events as presented for two exemplary days and regions for the Russian and Greenland blocking, respectively (Fig. 4c,d). While the southern gradient becomes positive (i.e., easterly geostrophic flow equatorward of the depicted region), the northern gradient becomes distinctively more negative compared to the climatology: at 500 hPa ΔZ_{N} exceeds -20 m/°lat over Russia in July and even -30 m/°lat over Greenland in March, further increasing upwards. Fig. 4c also shows some ΔZ_{S} profiles which do not reach the IB criterion at some grid cells within the depicted region. However, the all-mean gradients ΔZ_{S} and ΔZ_{N} clearly represent instantaneously blocked conditions during these particular days.

The corresponding evolution of the GPH gradients over time is shown in Fig. 5 for exemplary grid cells during the Russian and Greenland blocking, respectively. Different temporal and vertical behavior of ΔZ_{N} (Fig. 5a,b) and ΔZ_{S} (Fig. 5c,d) is evident. ΔZ_{N} is always negative in JJA 2010 and meets the IB criterion during almost the entire period. During some days in February and March 2013, however, it is positive in the entire troposphere, indicating a potential high pressure system at high northern latitudes (70°N to 75°N). In JJA 2010, the southern gradient is positive for a couple of days by end of June 2010 and for a longer time period from mid-July to mid-August 2010. In FMA 2013, positive ΔZ_{S} can be found for several days from mid-February to early March 2013 as well as for some days in early April 2013.

The comparison of the northern and the southern gradient and their combined use for IB detection based on the two blocking cases reveals that the ΔZ_{S} criterion is harder to meet than the ΔZ_{N} criterion, in particular during JJA 2010. During this time period two IB episodes can be identified over Russia: a short one end of June 2010 and a more persistent one from mid-July to mid-August 2010. Over Greenland, IB is found for mid-February to early March 2013 as well as for three days in early April 2013. Note that too short IB periods will not further appear as blocking since additional blocking criteria become effective. Overall, blocking episodes show a distinct vertical extent of the GPH gradient up to 300 hPa (Russia) and even up to the tropopause at about 200 hPa (Greenland). Outside blocked episodes the gradients mainly show climatological behavior.

The vertical structure of blocking in GPH and temperature anomalies during the Russian and Greenland blocking is shown in Fig. 6 and 7, repectively. Meridional cross sections reveal the longitudinal extent of blockings with strong positive GPH anomalies during these events (Fig. 6a,b). The different characteristics in their temporal evolution is shown in Fig. 6c and 6d. GPH anomalies extend into the stratosphere and show a maximum near the tropopause at approximately 200 hPa, exceeding 250 m to 300 m during blocking episodes. The height of the lapse-rate tropopause correlates well with GPH maxima and minima. During the persistent Russian blocking, it stays almost constant (Fig. 6c) compared to its usual variations during unblocked conditions. Meridional cross sections of temperature anomalies (Fig. 7a,b) reveal strong positive anomalies in the troposphere during blocking. These correspond to strong positive GPH anomalies and further result in a higher lapse-rate tropopause and in negative temperature anomalies in the stratosphere relative to climatological conditions. Strongest positive temperature anomalies of up to 10 K are found in the lower troposphere towards the surface during the Russian blocking (Fig. 7c). During the Greenland blocking, maximum temperature anomalies of up to 6 K are observed in the mid-troposphere (Fig. 7d).

5 Conclusions

We demonstrated the feasibility of atmospheric blocking detection in observations from radio occultation (RO). Utilizing about 800 profiles per day in the NH and applying an adequate gridding strategy, RO data are found dense enough to reasonably well resolve atmospheric variability on a daily basis as shown for geopotential height (GPH) fields and corresponding uncertainty measures.

For blocking detection we utilized a standard blocking detection algorithm based on GPH gradients at the 500 hPa pressure level. We analyzed two well-known blocking events over Russia in summer 2010 and over Greenland in late winter 2013. The resulting blocking pattern and temporal evolution in RO fields fully represent the characteristics of the events, consistent with existing literature.

Furthermore, we explored the vertically-resolved atmospheric structure during blocking based on tropospheric profiles of GPH gradients. While GPH gradient profiles during climatological condi-

tions are found smaller than 0 m/°lat in the entire troposphere above the boundary layer, indicating the westerly geostrophic flow at NH mid-latitudes, a clear separation between the northern and southern gradients is observed during blocking episodes. The southern gradients become positive, indicating an easterly geostrophic flow equatorwards, while the northern gradients become distinctively more negative up to a few -10 m/°lat, depending on region and season. A distinct vertical extent of these features up to 300 hPa and even up to the tropopause is found.

During blocking, characteristic structures in GPH and temperature anomaly fields are found in the troposphere and lower stratosphere. Strong GPH anomalies of up to 300 m in the upper troposphere yield a clear tropopause height increase. Corresponding temperature anomalies of up to 10 K are found in the middle and lower troposphere.

Overall, RO data are found very well suited for blocking detection and for providing information on the atmospheric structure during blocking episodes. They allow to detect and analyze vertically resolved atmospheric blocking patterns in a comprehensive observation-based record and a set of atmospheric variables comprising density, pressure, GPH, temperature, potential temperature, and tropospheric water vapor.

RO observations from constellations such as COSMIC cover the entire Earth, and can therefore provide a reliable data basis also in the Southern Hemisphere. They allow for comparisons of atmospheric characteristics of both hemispheres without being affected by inhomogeneous data coverage. Since RO profiles also sample the lower stratosphere, they can, moreover, provide valuable information about the influence of stratospheric phenomena on blocking. RO could therefore complement to ongoing research on the connection between sudden stratospheric warming events and blocking. Furthermore, combining RO observations in the free atmosphere with surface measurements will allow for a better understanding of the evolution of surface impacts, planned for future research.

Acknowledgements. The authors acknowledge ECMWF (Reading, UK) for access to its analysis data, and UCAR/CDAAC (Boulder, CO, USA) for access to its RO phase and orbit data. The WEGC processing team members, especially M. Schwärz, are thanked for OPSv5.6 RO data provision. RO data used for this study are available at WEGC (via www.wegcenter.at). We thank P. Davini (ISAC, IT), G. Kirchengast (WEGC, AT), and F. Ladstädter (WEGC, AT) for helpful comments and inputs. This work was funded by the Austrian Science Fund (FWF) under research grants W 1256-G15 (Doctoral Programme Climate Change – Uncertainties, Thresholds and Coping Strategies) and T 620-N29 (DYNOCC). We thank R. Anthes and one anonymous reviewer for their helpful comments and corrections.

References

Anstey, J. A., Davini, P., Gray, L. J., Woollings, T. J., Butchart, N., Cagnazzo, C., Christiansen, B., Hardiman, S. C., Osprey, S. M., and Yang, S.: Multi-model analysis of Northern Hemisphere winter blocking: Model biases and the role of resolution, J. Geophys. Res., 118, 3956–3971, doi:10.1002/jgrd.50231, 2013.

Anthes, R. A.: Exploring Earth's atmosphere with radio occultation: contributions to weather, climate, and space weather, Atmos. Meas. Tech., 4, 1077–1103, doi:10.5194/amt-4-1077-2011, 2011.

Barnes, E. A., Dunn-Sigouin, E., Masato, G., and Woollings, T.: Exploring recent trends in Northern Hemisphere blocking, Geophys. Res. Lett., 41, doi:10.1002/2013GL058745, 2014.

Barriopedro, D. and Calvo, N.: On the Relationship between ENSO, Stratospheric Sudden Warmings, and Blocking, J. Climate, 27, 4704–4720, doi:10.1175/JCLI-D-13-00770.1, 2014.

Barriopedro, D., García-Herrera, R., Lupo, A. R., and Hernández, E.: A climatology of northern hemisphere blocking, J. Climate, 19, 1042–1063, doi:10.1175/JCLI3678.1, 2006.

Barriopedro, D., García-Herrera, R., and Trigo, R. M.: Application of blocking diagnosis methods to General Circulation Models. Part I: a novel detection scheme, Climate Dyn., 35, 1373–1391, doi:10.1007/s00382-010-0767-5, 2010.

Biondi, R., Steiner, A. K., Kirchengast, G., and Rieckh, T.: Characterization of thermal structure and conditions for overshooting of tropical and extratropical cyclones with GPS radio occultation, Atmos. Chem. Phys., 15, 5181–5193, doi:10.5194/acp-15-5181-2015, 2015.

Brunner, L., Steiner, A. K., Scherllin-Pirscher, B., and Jury, M. W.: Feasibility of blocking detection in observations from radio occultation, in: Geophysical Research Abstracts, vol. 17, pp. EGU2015–1519, European Geoscience Union General Assembly 2015 (poster), 2015.

Cattiaux, J., Vautard, R., Cassou, C., Yiou, P., Masson-Delmotte, V., and Codron, F.: Winter 2010 in Europe: A cold extreme in a warming climate, Geophys. Res. Lett., 37, L20704, doi:10.1029/2010GL044613, 2010.

Cohen, J., Screen, J. A., Furtado, J. C., Barlow, M., Whittleston, D., Coumou, D., Francis, J., Dethloff, K., Entekhabi, D., Overland, J., and Jones, J.: Recent Arctic amplification and extreme mid-latitude weather, Nature Geoscience, 7, 627–637, doi:10.1038/ngeo2234, 2014.

Davini, P., Cagnazzo, C., Gualdi, S., and Navarra, A.: Bidimensional diagnostics, variability, and trends of Northern Hemisphere blocking, J. Climate, 25, 6496–6509, doi:10.1175/JCLI-D-12-00032.1, 2012.

Davini, P., Cagnazzo, C., and Anstey, J. A.: A blocking view of the stratosphere-troposphere coupling, J. Geophys. Res., 119, 11 100–11 115, doi:10.1002/2014JD021703, 2014a.

Davini, P., Cagnazzo, C., Fogli, P. G., Manzini, E., Gualdi, S., and Navarra, A.: European blocking and Atlantic jet stream variability in the NCEP/NCAR reanalysis and the CMCC-CMS climate model, Climate Dyn., 43, 71–85, doi:10.1007/s00382-013-1873-y, 2014b.

de la Torre, A. and Alexander, P.: Gravity waves above Andes detected from GPS radio occultation temperature profiles: Mountain forcing?, Geophys. Res. Lett., 32, L17815, doi:10.1029/2005GL022959, 2005.

Dee, D. P., Uppala, S. M., Simmons, A. J., Berrisford, P., Poli, P., Kobayashi, S., Andrae, U., Balmaseda, M. A., Balsamo, G., Bauer, P., Bechtold, P., Beljaars, A. C. M., van de Berg, L., Bidlot, J., Bormann, N., Delsol, C., Dragani, R., Fuentes, M., Geer, A. J., Haimberger, L., Healy, S. B., Hersbach, H., Hólm, E. V., Isaksen, L., Kållberg, P., Köhler, M., Matricardi, M., McNally, A. P., Monge-Sanz, B. M., Morcrette, J.-J., Park, B.-K., Peubey, C., de Rosnay, P., Tavolato, C., Thépaut, J.-N., and Vitart, F.: The ERA-Interim reanalysis:

configuration and performance of the data assimilation system, Quart. J. Roy. Meteor. Soc., 137, 553–597, doi:10.1002/qj.828, 2011.

Doblas-Reyes, F. J., Casado, M. J., and Pastor, M. A.: Sensitivity of the Northern Hemisphere blocking frequency to the detection index, J. Geophys. Res., 107, doi:10.1029/2000JD000290, 2002.

Foelsche, U., Scherllin-Pirscher, B., Ladstädter, F., Steiner, A. K., and Kirchengast, G.: Refractivity and temperature climate records from multiple radio occultation satellites consistent within 0.05 %, Atmos. Meas. Tech., 4, 2007–2018, doi:10.5194/amt-4-2007-2011, 2011.

Galarneau Jr., T. J., Hamill, T. M., Dole, R. M., and Perlwitz, J.: A Multiscale Analysis of the Extreme Weather Events over Western Russia and Northern Pakistan during July 2010, Mon. Wea. Rev., 140, 1639–1664, doi:10.1175/MWR-D-11-00191.1, 2012.

Gleisner, H., Thejll, P., Christiansen, B., and Nielsen, J. K.: Recent global warming hiatus dominated by low-latitude temperature trends in surface and troposphere data, Geophys. Res. Lett., 42, 510–517, doi:10.1002/2014GL062596, 2015.

Gorbunov, M. E., Benzon, H.-H., Jensen, A. S., Lohmann, M. S., and Nielsen, A. S.: Comparative analysis of radio occultation processing approaches based on Fourier integral operators, Radio Sci., 39, RS6004, doi:10.1029/2003RS002916, 2004.

Gramling, C.: Arctic impact, Science, 347, 818–821, doi:10.1126/science.347.6224.818, 2015.

Ho, S.-P., Hunt, D., Steiner, A. K., Mannucci, A. J., Kirchengast, G., Gleisner, H., Heise, S., von Engeln, A., Marquardt, C., Sokolovskiy, S., Schreiner, W., Scherllin-Pirscher, B., Ao, C., Wickert, J., Syndergaard, S., Lauritsen, K., Leroy, S., Kursinski, E. R., Kuo, Y.-H., Foelsche, U., Schmidt, T., and Gorbunov, M.: Reproducibility of GPS radio occultation data for climate monitoring: Profile-to-profile intercomparison of CHAMP climate records 2002 to 2008 from six data centers, J. Geophys. Res., 117, D18111, doi:10.1029/2012JD017665, 2012.

IPCC: Climate Change 2013: The Physical Science Basis. Contribution of Working Group I to the Fifth Assessment Report of the Intergovernmental Panel on Climate Change, Cambridge University Press, Cambridge, United Kingdom and New York, NY, USA, 2013.

Kursinski, E. R., Hajj, G. A., Schofield, J. T., Linfield, R. P., and Hardy, K. R.: Observing Earth's atmosphere with radio occultation measurements using the Global Positioning System, J. Geophys. Res., 102, 23 429–23 465, doi:10.1029/97JD01569, 1997.

Lejenäs, H.: Characteristics of southern hemisphere blocking as determined from a time series of observational data, Quart. J. Roy. Meteor. Soc., 110, 967–979, doi:10.1002/qj.49711046610, 1984.

Lhotka, O. and Kyselý, J.: Hot Central-European summer of 2013 in a long-term context, Int. J. Climatol., doi:10.1002/joc.4277, 2015.

Marques, R. d. F. C. and Rao, V. B.: Interannual variations of blockings in the southern hemisphere and their energetics, J. Geophys. Res., 105, 4625–4636, doi:10.1029/1999JD901066, 2000.

Martius, O., Polvani, L. M., and Davies, H. C.: Blocking precursors to stratospheric sudden warming events, Geophys. Res. Lett., 36, L14806, doi:10.1029/2009GL038776, 2009.

Matsueda, M.: Predictability of Euro-Russian blocking in summer of 2010, Geophys. Res. Lett., 38, L06801, doi:10.1029/2010GL046557, 2011.

Mattingly, K. S., McLeod, J. T., Knox, J. A., Shepherd, J. M., and Mote, T. L.: A climatological assessment of Greenland blocking conditions associated with the track of Hurricane Sandy and historical North Atlantic hurricanes, Int. J. Climatol., 35, 746–760, doi:10.1002/joc.4018, 2015.

Mendes, M. C. D. a., Trigo, R. M., Cavalcanti, I. F. A., and DaCamara, C. C.: Blocking Episodes in the Southern Hemisphere: Impact on the Climate of Adjacent Continental Areas, Pure and Applied Geophysics, 165, 1941–1962, doi:10.1007/s00024-008-0409-4, 2008.

Oliveira, F. N. M., Carvalho, L. M. V., and Ambrizzi, T.: A new climatology for Southern Hemisphere blockings in the winter and the combined effect of ENSO and SAM phases, Int. J. Climatol., 34, 1676–1692, doi:10.1002/joc.3795, 2014.

Peevey, T. R., Gille, J. C., Homeyer, C. R., and Manney, G. L.: The double tropopause and its dynamical relationship to the tropopause inversion layer in storm track regions, J. Geophys. Res., 119, 10,194–10,212, doi:10.1002/2014JD021808, 2014.

Pelly, J. L. and Hoskins, B. J.: A new perspective on blocking, J. Atmos. Sci., 60, 743–755, doi:10.1175/1520-0469(2003)060<0743:ANPOB>2.0.CO;2, 2003.

Pfahl, S., Schwierz, C., Croci-Maspoli, M., Grams, C. M., and Wernli, H.: Importance of latent heat release in ascending air streams for atmospheric blocking, Nature Geoscience, 8, 610–614, doi:10.1038/ngeo2487, 2015.

Pirscher, B., Foelsche, U., Borsche, M., Kirchengast, G., and Kuo, Y.-H.: Analysis of migrating diurnal tides detected in FORMOSAT-3/COSMIC temperature data, J. Geophys. Res., 115, D14108, doi:10.1029/2009JD013008, 2010.

Quiroz, R. S.: The association of stratospheric warmings with tropospheric blocking, J. Geophys. Res., 91, 5277–5285, doi:10.1029/JD091iD04p05277, 1986.

Randel, W. J. and Wu, F.: Kelvin wave variability near the equatorial tropopause observed in GPS radio occultation measurements, J. Geophys. Res., 110, D03102, doi:10.1029/2004JD005006, 2005.

Randel, W. J. and Wu, F.: Variability of Zonal Mean Tropical Temperatures Derived from a Decade of GPS Radio Occultation Data, J. Atmos. Sci., 72, 1261–1275, doi:10.1175/JAS-D-14-0216.1, 2015.

Randel, W. J., Wu, F., and Ríos, W. R.: Thermal variability of the tropical tropopause region derived from GPS/MET observations, J. Geophys. Res., 108, doi:10.1029/2002JD002595, 2003.

Rex, D. F.: Blocking Action in the Middle Troposphere and its Effect upon Regional Climate I: An aerological study of blocking action, Tellus, 2, 196–211, doi:10.1111/j.2153-3490.1950.tb00331.x, 1950.

Rieckh, T., Scherllin-Pirscher, B., Ladstädter, F., and Foelsche, U.: Characteristics of tropopause parameters as observed with GPS radio occultation, Atmos. Meas. Tech., 7, 3947–3958, doi:10.5194/amt-7-3947-2014, 2014.

Scherllin-Pirscher, B., Kirchengast, G., Steiner, A. K., Kuo, Y.-H., and Foelsche, U.: Quantifying uncertainty in climatological fields from GPS radio occultation: an empirical-analytical error model, Atmos. Meas. Tech., 4, 2019–2034, doi:10.5194/amt-4-2019-2011, 2011a.

Scherllin-Pirscher, B., Steiner, A. K., Kirchengast, G., Kuo, Y.-H., and Foelsche, U.: Empirical analysis and modeling of errors of atmospheric profiles from GPS radio occultation, Atmos. Meas. Tech., 4, 1875–1890, doi:10.5194/amt-4-1875-2011, 2011b.

Scherllin-Pirscher, B., Deser, C., Ho, S.-P., Chou, C., Randel, W., and Kuo, Y.-H.: The vertical and spatial structure of ENSO in the upper troposphere and lower stratosphere from GPS radio occultation measurements, Geophys. Res. Lett., 39, L20801, doi:10.1029/2012GL053071, 2012.

Scherllin-Pirscher, B., Steiner, A. K., and Kirchengast, G.: Deriving dynamics from GPS radio occultation: Three-dimensional wind fields for monitoring the climate, Geophys. Res. Lett., 41, 7367–7374, doi:10.1002/2014GL061524, 2014.

Scherrer, S. C., Croci-Maspoli, M., Schwierz, C., and Appenzeller, C.: Two-dimensional indices of atmospheric blocking and their statistical relationship with winter climate patterns in the Euro-Atlantic region, Int. J. Climatol., 26, 233–249, doi:10.1002/joc.1250, 2006.

Schmidt, T., Heise, S., Wickert, J., Beyerle, G., and Reigber, C.: GPS radio occultation with CHAMP and SAC-C: global monitoring of thermal tropopause parameters, Atmos. Chem. Phys., 5, 1473–1488, doi:10.5194/acp-5-1473-2005, 2005.

Schmidt, T., Wickert, J., Beyerle, G., and Heise, S.: Global tropopause height trends estimated from GPS radio occultation data, Geophys. Res. Lett., 35, L11806, doi:10.1029/2008GL034012, 2008.

Schwärz, M., Scherllin-Pirscher, B., Kirchengast, G., Schwarz, J., Ladstädter, F., Fritzer, J., and Ramsauer, J.: Multi-Mission Validation by Satellite Radio Occultation, Final report for ESA/ESRIN No. 01/2013, WEGC, University of Graz, Austria, 2013.

Schwierz, C., Croci-Maspoli, M., and Davies, H. C.: Perspicacious indicators of atmospheric blocking, Geophys. Res. Lett., 31, L06125, doi:10.1029/2003GL019341, 2004.

Shepherd, T. G.: Atmospheric circulation as a source of uncertaintyin climate change projections, Nature Geoscience, 7, 703–708, doi:10.1038/ngeo2253, 2014.

Sillmann, J., Croci-Maspoli, M., Kallache, M., and Katz, R. W.: Extreme Cold Winter Temperatures in Europe under the Influence of North Atlantic Atmospheric Blocking, J. Climate, 24, 5899–5913, doi:10.1175/2011JCLI4075.1, 2011.

Steiner, A. K., Lackner, B. C., Ladstädter, F., Scherllin-Pirscher, B., Foelsche, U., and Kirchengast, G.: GPS radio occultation for climate monitoring and change detection, Radio Sci., 46, RS0D24, doi:10.1029/2010RS004614, 2011.

Steiner, A. K., Hunt, D., Ho, S.-P., Kirchengast, G., Mannucci, A. J., Scherllin-Pirscher, B., Gleisner, H., von Engeln, A., Schmidt, T., Ao, C., Leroy, S. S., Kursinski, E. R., Foelsche, U., Gorbunov, M., Heise, S., Kuo, Y.-H., Lauritsen, K. B., Marquardt, C., Rocken, C., Schreiner, W., Sokolovskiy, S., Syndergaard, S., and Wickert, J.: Quantification of structural uncertainty in climate data records from GPS radio occultation, Atmos. Chem. Phys., 13, 1469–1484, doi:10.5194/acp-13-1469-2013, 2013.

Sun, D.-Z., Zhang, T., Sun, Y., and Yu, Y.: Rectification of El Niño–Southern Oscillation into Climate Anomalies of Decadal and Longer Time Scales: Results from Rorced Ocean GCM Experiments, J. Climate, 27, 2545–2561, doi:10.1175/JCLI-D-13-00390.1, 2014.

Tibaldi, S. and Molteni, F.: On the operational predictability of blocking, Tellus A, 42, 343–365, doi:10.1034/j.1600-0870.1990.t01-2-00003.x, 1990.

Tibaldi, S., Tosi, E., Navarra, A., and Pedulli, L.: Northern and southern hemisphere seasonal variability of blocking frequency and predictability, Mon. Wea. Rev., 122, doi:10.1175/1520-0493(1994)122<1971:NASHSV>2.0.CO;2, 1994.

Tsuda, T.: Characteristics of atmospheric gravity waves observed using the MU (Middle and Upper atmosphere) radar and GPS (Global Positioning System) radio occultation, Proc. Jpn. Acad., Ser. B, 90, 12–27, 2014.

von Engeln, A., Teixeira, J., Wickert, J., and Buehler, S. A.: Using CHAMP radio occultation data to determine the top altitude of the Planetary Boundary Layer, Geophys. Res. Lett., 32, L06815, doi:10.1029/2004GL022168, 2005.

Wiedenmann, J. M., Lupo, A. R., Mokhov, I. I., and Tikhonova, E. A.: The climatology of blocking anticyclones for the northern and southern hemispheres: block intensity as a diagnostic, J. Climate, 15, 3459–3473, doi:10.1175/1520-0442(2002)015<3459:TCOBAF>2.0.CO;2, 2002.

Woollings, T., Charlton-Perez, A., Ineson, S., Marshall, A. G., and Masato, G.: Associations between stratospheric variability and tropospheric blocking, J. Geophys. Res., 115, D06108, doi:10.1029/2009JD012742, 2010.

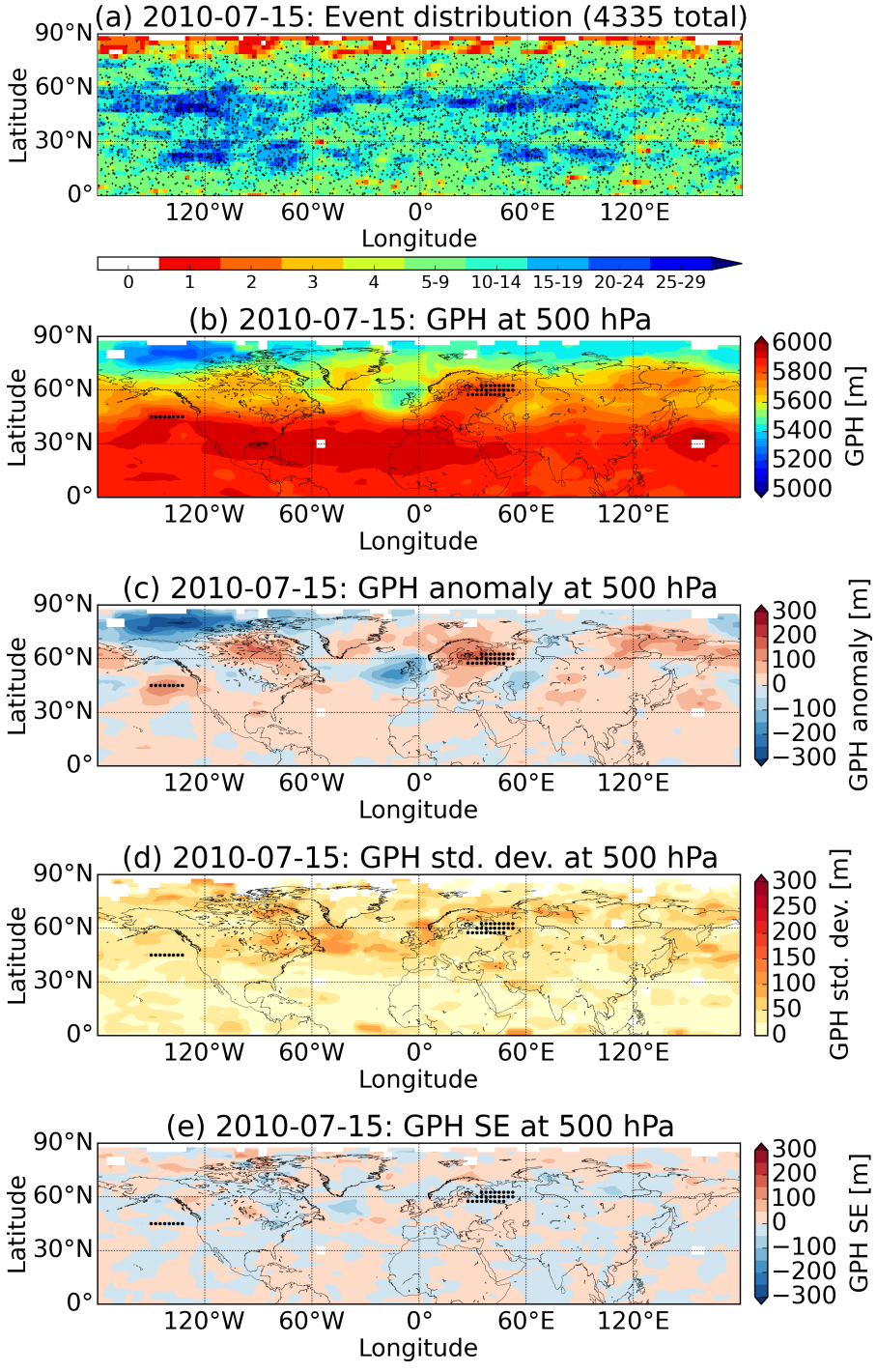

Figure 1. (a) RO event distribution (plus signs) in the NH for an exemplary day (±2 neighboring days) during the Russian blocking and number of events per grid cell (shading). Geographic maps at 500 hPa of (b) GPH, (c) GPH anomaly relative to the mean from 2006 to 2013, (d) standard deviation of individual profiles, and (e) sampling error. Blocked grid cells are indicated by dots, missing data are white.

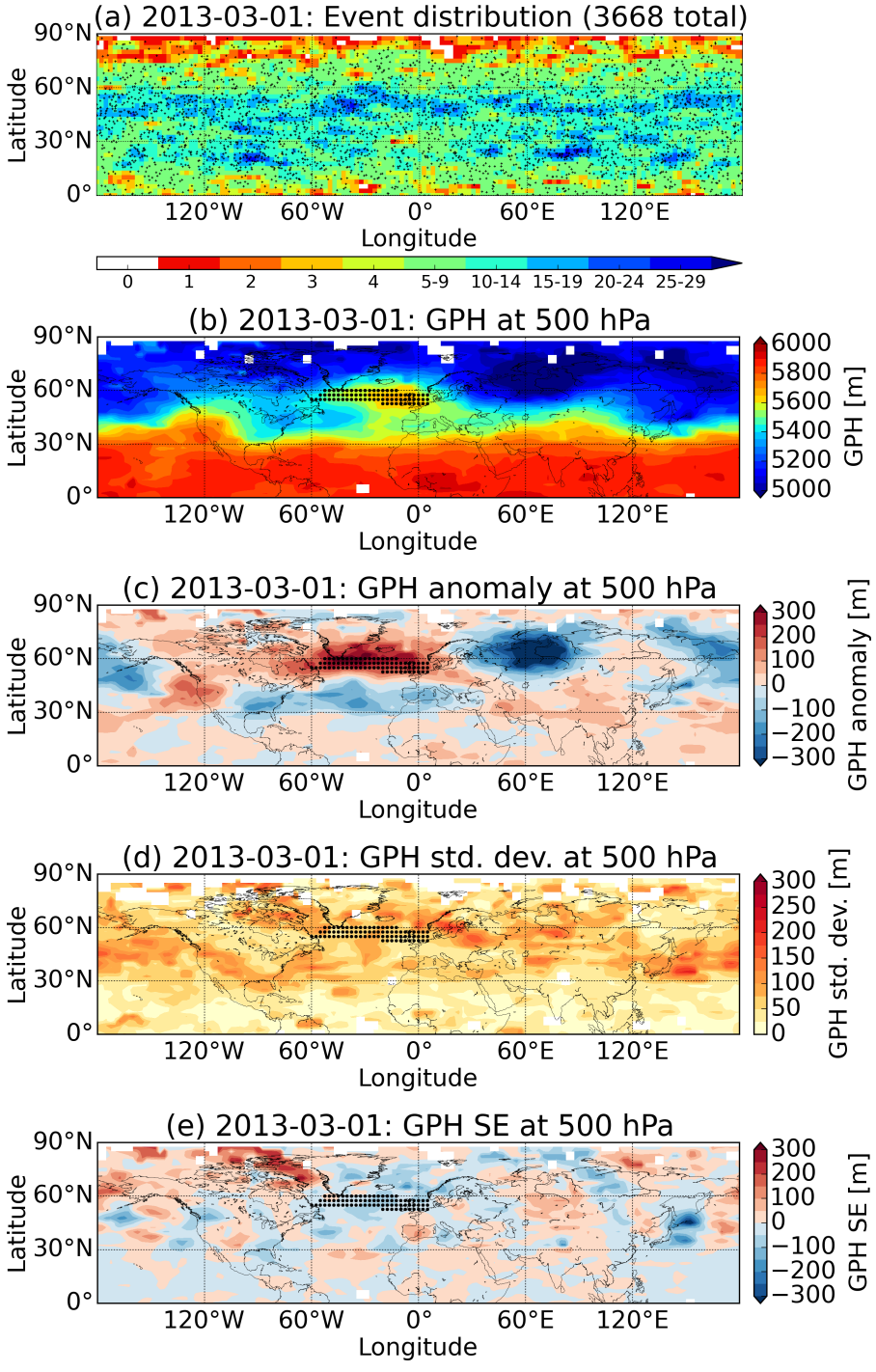

Figure 2. Same layout as Fig. 1 but for an exemplary day during the Greenland blocking.

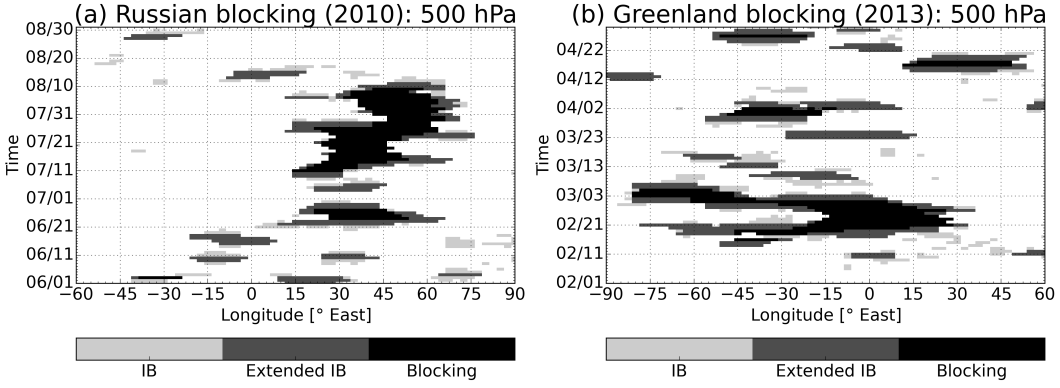

Figure 3. Hovmöller diagrams of observed blocking occurrence at 500 hPa over (a) Russia in JJA 2010 and over (b) Greenland in FMA 2013. Blocking is considered between 50°N and 65°N. Shading indicates the three blocking detection steps, IB (light gray), extended IB (dark gray), and blocking (black).

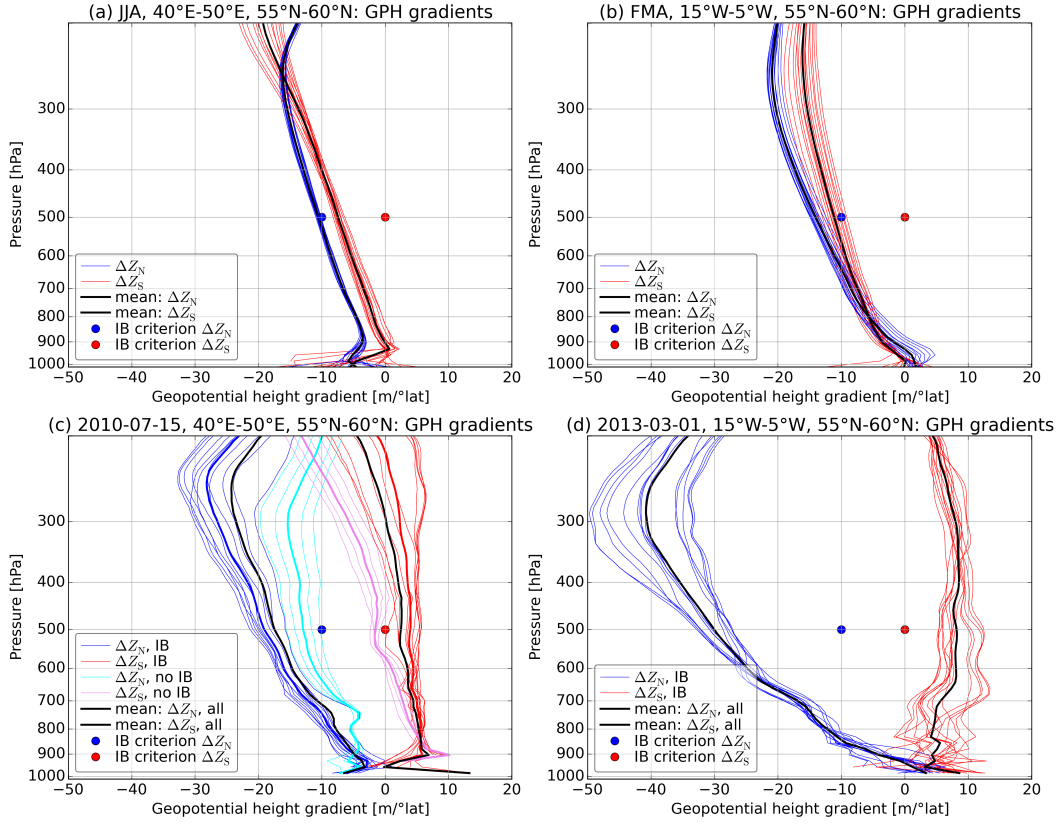

Figure 4. Vertical profiles of (blue) ΔZ_{N} and (red) ΔZ_{S} during climatological conditions in (a) JJA 2006 to 2013 within 40°E to 50°E and 55°N to 60°N, and (b) FMA 2006 to 2013 within 15°W to 5°W and 55°N to 60°N. ΔZ_{N} and ΔZ_{S} for individual grid cells (thin lines) and the respective region-mean (bold lines). IB blocking criteria at 500 hPa for ΔZ_{N} (blue dot) and ΔZ_{s} (red dot). Vertical profiles of GPH gradients for an exemplary day during the (c) Russian blocking and (d) Greenland blocking, same area as (a) and (b), respectively. Blocked profiles (blue, red) and those not meeting the blocking criteria (light blue, light red). Mean (bold colored) and all-mean (bold black) ΔZ_{N} and ΔZ_{S} profiles. Note that the mean is identical with the all-mean for the Greenland blocking.

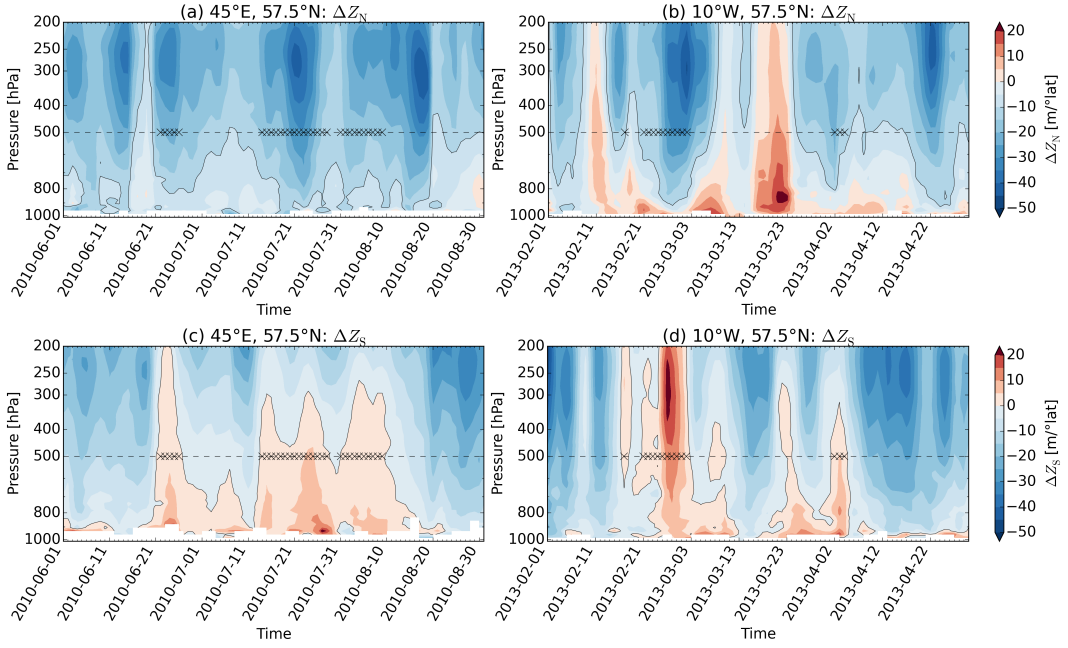

Figure 5. Temporal evolution of ΔZ_{N} and ΔZ_{S} during the (a,c) Russian and (b,d) Greenland blocking. Blocking criteria (solid black contours) are indicated as (a,b) $-10\,\mathrm{m}/^{\circ}\mathrm{lat}$ for ΔZ_{N} and (c,d) $0\,\mathrm{m}/^{\circ}\mathrm{lat}$ for ΔZ_{S}. IB (crosses) is indicated at the 500 hPa pressure level (dashed black line).

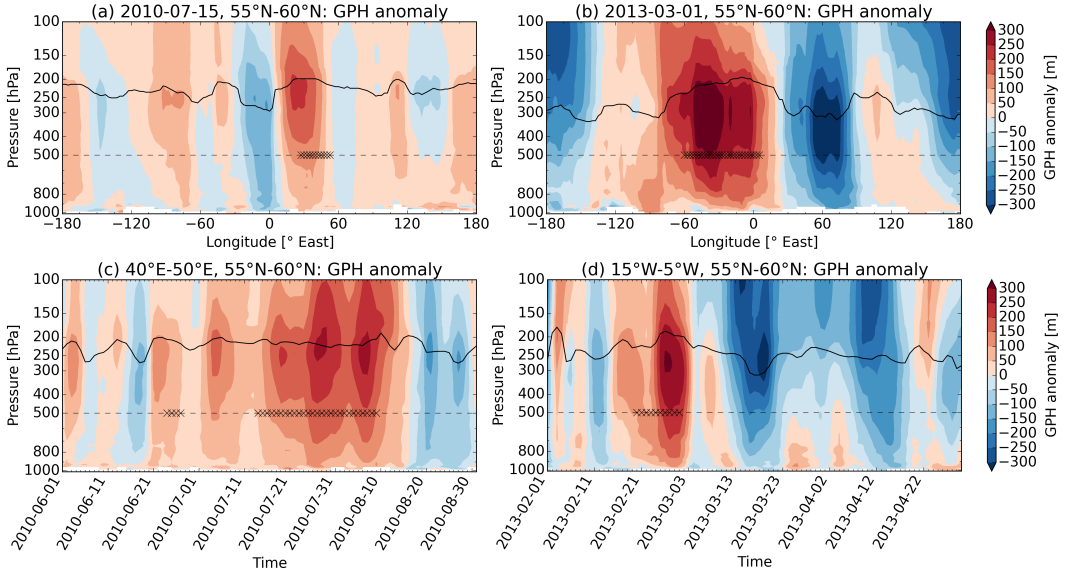

Figure 6. GPH anomalies during (left column) Russian blocking and (right column) Greenland blocking. (a,b) Meridional cross sections of GPH for two exemplary days and regions as well as (c,d) temporal evolution of GPH for the same regions. Blocking (crosses) at the 500 hPa level (dashed line) is indicated if at least one grid cell in the averaged area is blocked. The solid line denotes the lapse-rate tropopause.

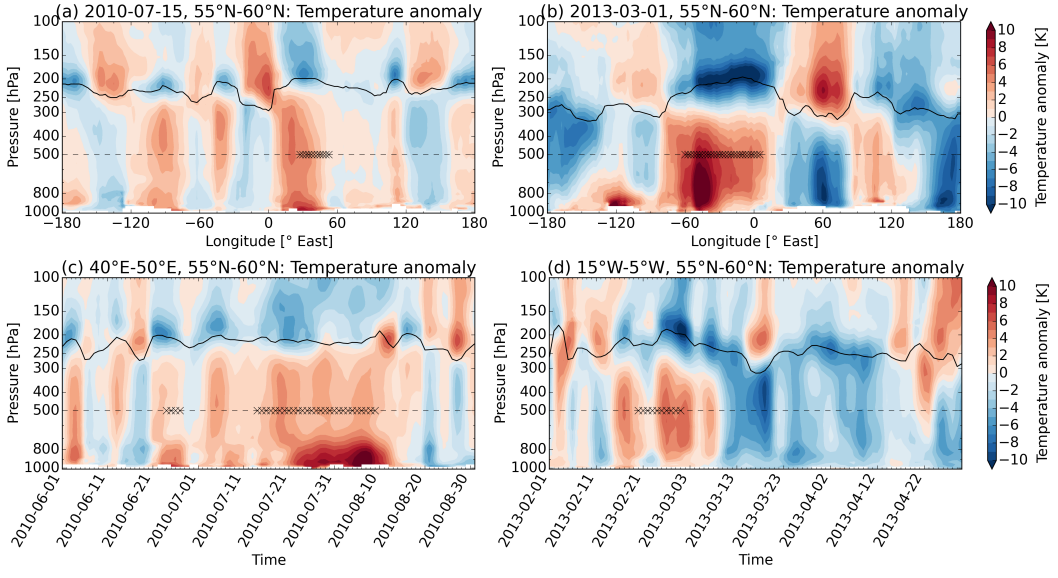

Figure 7. Same layout as Fig. 6 but for temperature anomalies.